Visual Abstract

Corrosion behavior of Shape Memory Alloy in NaCl environment and deformation recovery maintenance in Cu-Zn-Al system

Andrea Brotzu
Department of Chemical Engineering, Material, Environments (DICMA) Sapienza, University of Rome (Italy)
andrea.brotzu@uniroma1.it, http://orcid.org/0000-0001-9530-4602

Barbara De Filippo
Consiglio Nazionale delle Ricerche, Istituto per le Applicazioni del Calcolo "Mauro Picone", Rome (Italy)
barbara.defilippo@cnr.it, http://orcid.org/ 0000-0002-9387-0122

Stefano Natali, Laura Zortea
Department of Chemical Engineering, Material, Environments (DICMA) Sapienza, University of, Rome (Italy)
stefano.natali@uniroma1.it, https://orcid.org/0000-0002-2742-0270
laura.zortea@uniroma1.it, htttp://orcid.org/0000-0002-2200-5051

ABSTRACT. Shape memory effect (SME) and the relation with corrosion behavior of Cu-Zn-Al Smart Memory Alloys (SMAs) were investigated using different techniques: Scanning Electron Microscopy equipped with an Energy Dispersive System, X-Ray Diffraction analysis, Electrochemical Test in NaCl solutions with different concentrations (0.035%, 0.35% and 3.5%), which simulate coastal conditions, mechanical characterization through tensile test and guided bend test.
SMAs are an important class of smart materials able to recover after deformation a pre-imposed shape through a temperature modification. These alloys show great potential, finding several applications in medicine and in different types of industry sectors (aerospace, architecture, automotive etc.). Cu-based SMAs, including Cu-Zn-Al alloys, have lower production costs with respect to Ni-Ti alloys as well as good possibility in seismic and architectural applications. A Cu-Zn-Al alloy with a theoretical composition of 25 wt.% Zn and 4 wt.% Al was produced by casting method.
The aim of this study is to characterize the microstructure, the mechanical properties and the corrosion behavior through different kind of standard corrosion tests of this alloy and to evaluate the effect of corrosion damage on the shape memory recovery capability through a combination of corrosion and thermo-mechanical cyclic test and SEM observations.

KEYWORDS. Cu-Zn-Al alloy; Shape memory effect; Electrochemical test; Corrosion; Shape recovery.

OPEN ACCESS

Citation: Brotzu, A., De Filippo, B., Natali, S., Zortea, L.., Corrosion behavior of Shape Memory Alloy in NaCl environment and deformation recovery maintenance in Cu-Zn-Al system, Frattura ed Integrità Strutturale, xx (2022) 64-74.

Received: 09.05.2022
Accepted: 21.07.2022
Online first: 28.07.2022
Published: 01.10.2022

Copyright: © 2022 This is an open access article under the terms of the CC-BY 4.0, which permits unrestricted use, distribution, and reproduction in any medium, provided the original author and source are credited.

INTRODUCTION

Shape Memory Alloys (SMAs), together with Super Elastic alloys (SEAs), are a class of metallic materials with specific mechanical characteristics. They can absorb high levels of deformation and return to its pre-deformed macroscopic form through a solid phase transformation thermally activated. The solid phase transformation is a reversible crystallographic phenomenon, and it is due to the shift from austenite (phase stable at high temperature) to martensite (phase stable at lower temperature) through a lattice deformation and vice versa [1, 2]. Shape Memory Effect (SME) or Super Elastic Effect (SEE) is deeply connected to transformation temperatures (A_f, A_s, M_s and M_f), which determine the stable phase at operating temperature [3]. In the martensite field at operation temperature the alloy can express the memory effect, otherwise, the austenite phase will generate a super elastic effect [4]. Both SME and SEE are explored in Smart Materials, and this made them appropriate for several uses. Among Smart Materials, SMAs are gaining importance in many different engineering fields from aerospace to biomedical ones, including automotive and architecture applications [5].
Shape memory transformation is observed in many metallic systems [6]. The main systems identified, in addition to the well-known and studied equiatomic nickel-titanium system (Ni-Ti), are the iron-based alloy (Fe-Mn-Si, Fe-Mn-Cr-Si) and the copper-based alloys (Cu-Al, Cu-Al-Mn, Cu-Al-Ni Cu-Be) and between them the Cu-Zn-Al system [7,8]. Cu-Zn-Al alloys, underdeveloped in the past due to poor control of transformation temperatures and to the intrinsic alloy brittleness which is linked to the high grain dimensions usually obtained [7], are a class of smart metals able to develop both one-way or two-way in SME and in SEE as well [9]. These Cu alloys now have various proposed applications in engineering and seismic fields, thanks to their intrinsic characteristics which consist of being cost-effective products and easily produced [8, 10].
Theoretical research about these smart materials must follow many different but necessary paths to provide essential tools for engineers to be able to carry out designs that cover their use. It is necessary to investigate all possible aspects and thoroughly understand the physical, mechanical, and chemical behavior of these new materials before proposing commercial use.
One of the less studied aspects for these materials is the corrosion behavior with respect to the shape memory conservation. Corrosion of structural materials can be considered one of the major material worldwide losses; this undesired behavior causes damage for about a 3-4% of the Gross National Income of developed countries [11], and it's very pronounced at coastal conditions, where the usual corrosion factors are magnified by high humidity and air salinity [12]. For this new class of materials, the up to now consolidated use doesn't require a design which considers the corrosion resistance. Instead, the new proposed fields of applications, which contemplate their use in different and potentially dangerous environments, require a deep knowledge of their corrosion behavior in environments similar to natural ones. Moreover, it is not sufficient to characterize the usual corrosion parameters like the corrosion rate evaluation and the potentiodynamic behavior, but, considering that their mechanical properties arise from a phase transformation, it is also important to evaluate how the corrosion process can influence or can be influenced by this transformation.
In this study the microstructure, the mechanical properties, and the corrosion behavior in simulated coastal environments (solution of NaCl in water at different concentrations) of a Cu-Zn-Al SMA are addressed. The work also analyzes how the specific mechanical properties of Cu-Zn-Al SMAs can be affected by corrosive attack with the aim to investigate what happens to the material surface damaged when subjected to deformation. In particular it has been evaluated how the corrosion defects evolve in cracks after a mechanical solicitation, the influence of the deformation level on the cracks number and length and if they grow during the cyclic deformation/shape recovery.

EXPERIMENTAL

Material production and metallographic investigation

For this work a SMA Cu-Zn-Al alloy was produced in laboratory scale. Pure electrolytic copper (99.5%,) chemical grade zinc (99.995%) and aluminum 1100 were used as raw materials. Pure metals were melted in a centrifugal induction furnace under argon protective atmosphere and then cast in a graphite mold. The target composition is Zn 25% wt, Al 4%wt, Cu balance. The Cu-Zn-Al ingot was cut employing a diamond blade to obtain several samples with dimensions of 33mmx10mmx1mm for microstructure analysis, mechanical and corrosion tests.
The composition was measured using the EDS system KEVEX Noran System six. The material was tested in as cast condition.
The microstructures were characterized by optical microscope observation on sample grounded with SiC papers up to 1200 mesh, polished up to 0.3 μm alumina suspensions and etched with a ferric chloride acid solution (ferric chloride 3 g, HCl 10 ml, Ethanol 90 ml) in order to highlight grain boundary morphologies and martensitic microstructure. XRD

measurements were made with a X-PERT Diffractometer equipped with a Philips vertical Bragg–Brentano powder goniometer. A step–scan mode was used in the 2θ range from 35° to 100° with a step width of 0.02° and a counting time of 1.5 s per step. The employed radiation was mono-chromated Cu Kα.

Electrochemical test

The tests were performed at 20°C in open air in a cell containing different concentrations of NaCl solutions (0.035%, 0.35% and 3.5%) by using a PARSTAT 3 potentiostat/galvanostat (Princeton Applied Research). A classical three-electrode configuration was used in the experimentation for potentiodynamic test, where the reference electrode was a saturated calomel electrode (SCE). The counter electrode was made of platinum and the specimen was the working electrode.
Potentiodynamic tests were carried out according to ASTM G5 standard. Scan rate is 0.1666 mV/s, step 6 s, potential range is OCP -0.25 ÷ Ref +1V, exposed surface 2 cm^2. Samples were immersed in testing solutions 30 minutes before starting analysis. Open Circuit Potential (OCP) was measured for 600 s.
Tafel parameters were measured on potentiodynamic tests carried out with the following parameters: scan rate 0.16666 mV/s, step 3 s, potential range OCP -0.25 V ÷ OCP +0.25 V, exposed surface 2 cm^2.
Linear Potential Resistance (LPR) was measured on potentiodynamic test carried out with the following parameters: scan rate 0.1666 mV/s, step 0.6 s, potential range OCP -20 mV ÷ OCP +20 mV, exposed surface 2 cm^2.

Mechanical characterization

In order to evaluate the SMA mechanical properties a tensile test was carried out according to ASTM E 8M standard.
The sample geometry was: rectangular section (1x6 mm), L_0=13.8 mm, L_c=15 mm.
The test parameters were: crosshead speed was 0.5 mm/min with an estimated deformation rate of 2.8%/min, acquisition rate 10 points/s, load cell 30 kN, testing machine Instron 3367.
Shape memory capacity after corrosion processes was measured through guided-bend tests, according to ASTM E290. The specimen dimensions were: L=33.15mm, W= 9.5 mm, T= 1 mm (Fig. 1a).
The testing parameters were: crosshead speed 0.5 mm/min, distance between lower supports 20 mm, plunger diameter 6 mm. Bending specimens were corroded in the central area (total area 2 cm^2) through a potentiostatic test (applied tension 100 mV over OCP for 30 min, solution 0.035% NaCl). The corroded surface was characterized through SEM observations.
The corroded sample was subjected to the following thermo-mechanical cycle:
- guided-bend deformations with a fixed maximum plunger shift
- measurements of the bending angle under load (Fig. 1b)
- measurements of the bending angle without load in order to evaluate the elastic recovery (Fig. 1c)
- heating of the deformed sample at 70 °C for 1 min (immerging the sample in a thermostatic bath)
- measurement of the final bending angle (deformation recovered by shape memory effect, Fig. 1d)

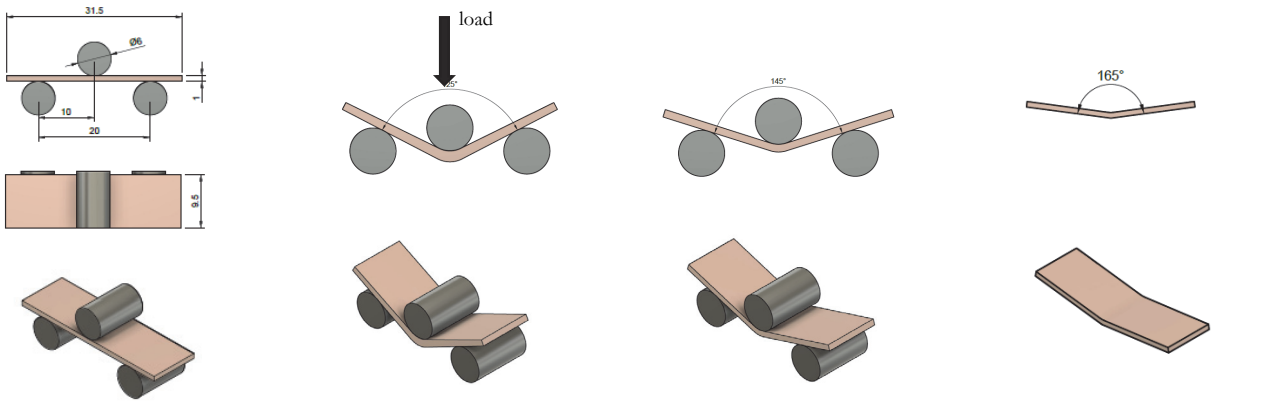

a). Guided bed test design

b) sample bended with the maximum plunger shift (with the load applied)

c) sample after load removal (sample elastic recovery)

d) Sample after the heat treatment for the shape memory effect

Figures 1 (a-d): Guided-bend test schematic description.

The described cycle was repeated 25 times applying a plunger shift of 5 mm, 25 times with a shift of 6 mm, 25 times with a shift of 7 mm, 1 time applying 10 mm. SEM observations were carried out on the corroded surface (where tensile stress was applied) to evaluate the evolution of superficial cracks which could be produced starting from the corrosion defects.

RESULTS AND DISCUSSION

Microstructural characteristic of Cu-Zn-Al

Microstructural analyses were carried out on several specimens. Fig. 2a shows the microstructure of tested alloy, where a relative coarse grain structure can be observed. These grains are characterized by an internal needle-like structure typical of martensitic phases. Some austenitic areas are also detected. On the grain boundary a secondary phase can be observed (Fig. 2b), in these areas coarse equi-oriented needle microstructures appear. They grow from the boundary to the center of the grain, always with the same inclination/orientation. The EDS microanalysis carried out on these secondary phases doesn't point out any difference with the composition of the central area of the grain. Their low quantity and their reduced dimensions don't allow to define which kind of phase they could be. In previous works it has been observed that these microstructures tend to disappear with a homogenization thermal treatment which is usually done to reduce the amount of residual austenite and to consequently maximize the shape memory effect. This treatment generally consists in heating the material at a temperature where it is fully monophasic (β phase). Considering the Zn equivalent of the studied alloy (39.5%w) and the Cu-Zn phase diagram, it is fully β at temperatures above 800 °C. The heat treatment time depends to sample thickness. The time must be the shortest possible to avoid an excessive enlargement of the grain. After heating the alloy can be cooled at different cooling rate (air cooling, quenching in hot, cold or ice water, liquid nitrogen quenching). In the previous work a temperature of 850°C has been selected followed by liquid nitrogen quenching. This heat treatment maximizes the quantity of martensitic phase and the second phase observed at the grain boundary disappears. This microstructure is confirmed by the XRD analysis (Fig. 3). The diffractogram shows a great number of peaks just observed in previous works [8, 13-15] on Cu-Zn-Al SMA alloys. Almost all are those of the martensitic structures. Only the highlighted peak can be referred to the austenitic phase. Tab. 1 shows the relative chemical composition of the material.

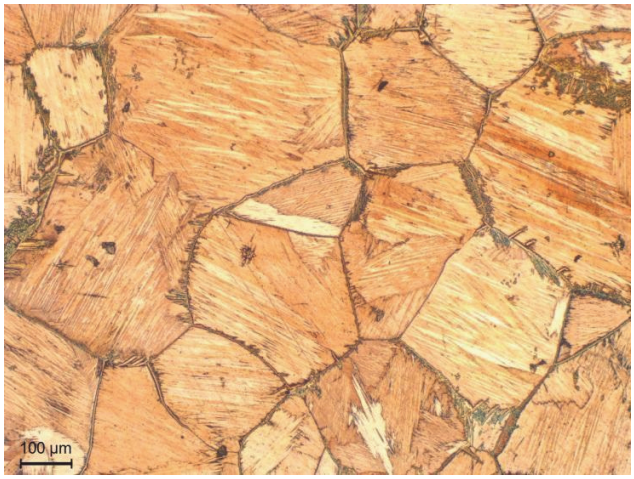

Figure 2a: Alloy microstructure after ferric chloride metallographic etch.

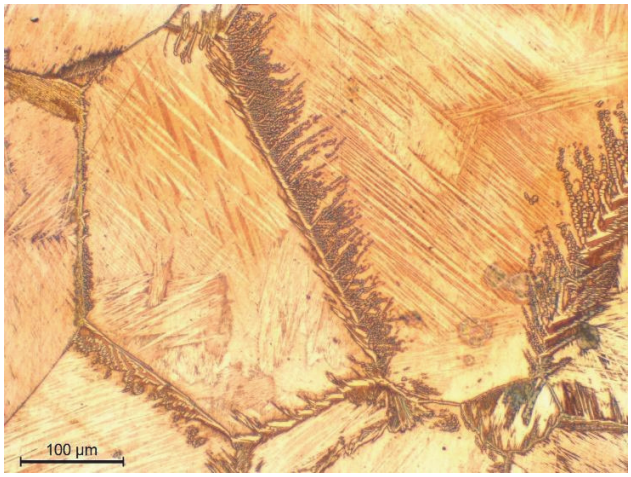

Figure 2b: Alloy microstructure after ferric chloride metallographic etch coarse-equioriented needle microstructure.

	Cu %w	Zn %w	Al %w	Cu %a	Zn %a	Al %a
Average value	70.80	25.80	3.40	68.17	24.17	7.66
Standard deviation	0.45	0.77	0.60	1.01	0.58	1.04

Table 1 Alloy chemical composition (EDS analysis).

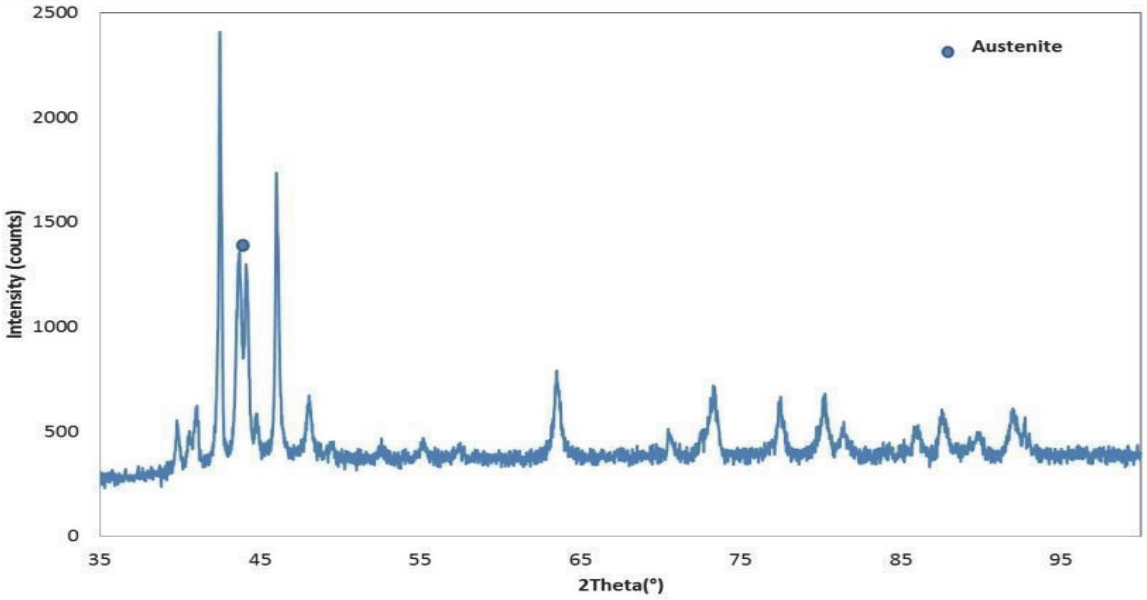

Figure 3: XRD diffractogram of the tested Cu-Zn-Al alloy, austenite and martensite picks were detected.

Mechanical test

Fig. 4 shows the typical stress-strain curve of the studied SMA, where the breaking elongation is in the range of 6%-10% and the σ_{max} is 425-440 MPa. The difference in the elongation could be due to the inner shrinkage defect observed in the central area of the specimens. This defect arises from the mold design which produces an internal shrinkage during the solidification phase, Fig. 5 shows the fracture surface morphology. The fracture surface points out a brittle fracture behavior. It appears predominantly intergranular with a crack path which surrounds the SMA grains. Some areas where the fracture surface show the characteristic plastic fracture dimple. Probably the crack grows along the brittle martensitic grain boundary and occasionally cut the more plastic austenitic grains sometimes observed in the microstructure.

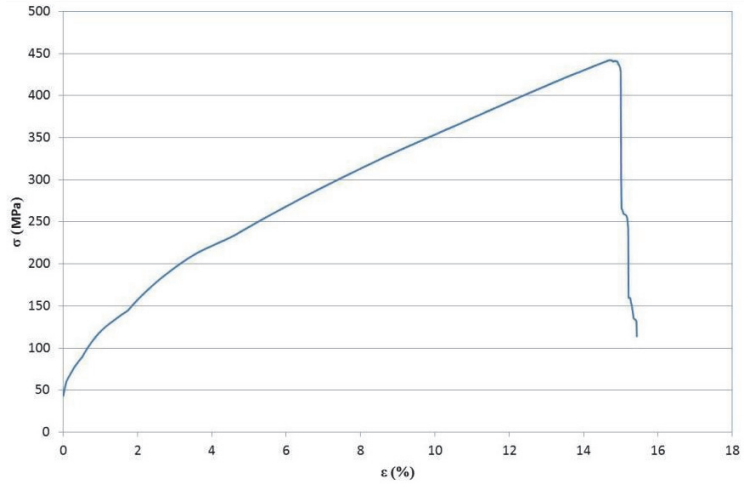

Figure 4: Stress-strain curve of the tested SMA.

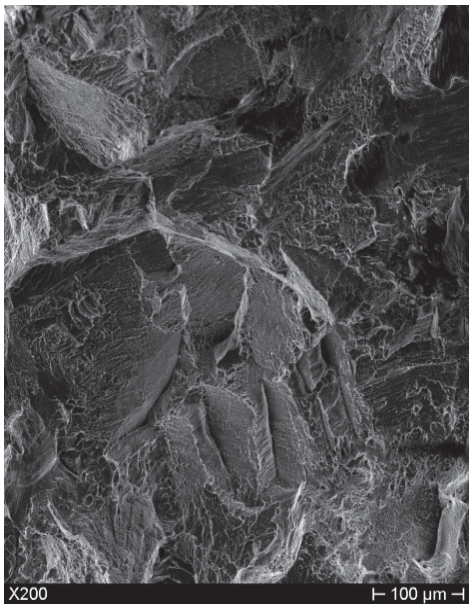

Figure 5: SEM observation of the tested Cu-Zn-Al alloy.

Electrochemical test

Fig. 6 shows the potentiodynamic tests carried out in solution with different concentrations. These tests were done after the Open Circuit Potential (OCP) measurements (Fig. 7). In order to complete the corrosion study in the same conditions more detailed scansions in the proximity of the free corrosion potential were carried out. Tafel parameters and Linear Polarization Results (LPR) were evaluated. The parameters of all the corrosion tests are reported in section "Experimental-Electrochemical test". Tab. 2 reports the results of the Tafel test (β_{anodic} and $\beta_{cathodic}$) and those of the LPR test (E_{corr} e I_{corr}). Tab. 3 reports a comparison between the corrosion parameters (E_{corr} e I_{corr}) evaluated through the analysis of the different corrosion tests.

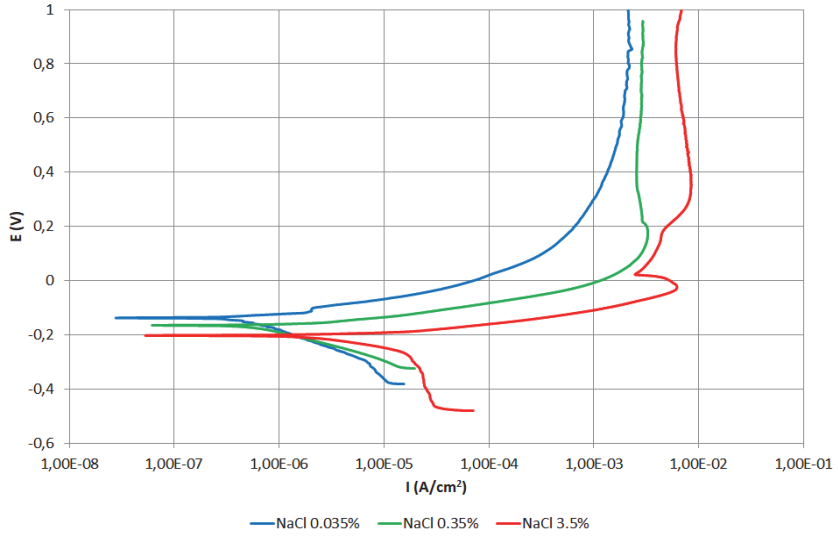

Figure 6: Potentiodynamic tests carried out on samples at different NaCl solution concentrations (in blue 0.035%, in green 0.035% and in red 3.5%).

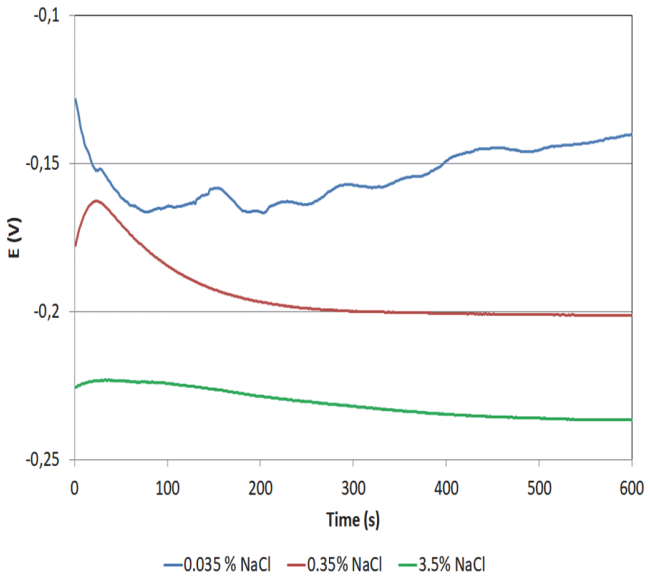

Figure 7: Open Circuit Potential (OCP) plot.

The OCP and the free corrosion potential (E_{corr}) decreases as the NaCl concentration increases. They pass from value around -140 mV measured in NaCl 0.035 $\%_w$ solution, to -190 ÷ -200 mV in 0.35 NaCl $\%_W$ solution, to -210 ÷ -240 in NaCl 3.5$\%_w$ solution.

Corrosion density currents were quite similar in the more concentrated solutions. In these environments their values were in the range of 2.3 ÷ 3.7 10^{-06} A/cm^2. Lower currents values were measured in the lower concentrated solution (1.8÷5.7 10-

07 A/cm²). Also, the shape of the potentiodynamic plot is different. In the more concentrated solutions, the corrosion currents reach a maximum value when the potential is around 0 V vs. reference electrode, and then they stabilize with the potential rising at a value comprised between 2.5 and 3.5 10^{-03} A/cm². This behavior, similar to a passivation process, is linked to the development of a compact layer of copper salts (usually atacamite ($CuCl2(OH)_3$) produced by the corrosion process on the surface. This layer stabilizes the corrosion rate because the corrosive process is in this case mainly influenced by diffusion processes of the involved chemical species between the copper salt layer. In lower concentrated solution a continuous rising of the corrosion current is observed, at high potential the current reaches values similar to those observed in more concentrated solutions.

NaCl %	Rp (kOhm)	Beta cathodic (mV)	Beta anodic (mV)	I corr (A/cm²)
0.035	15.234	160.67	54.502	5.8 E-07
0.35	2.411	71.40	62.26	2.61. E-06
3.5	1.957	75.71	33.24	2.23 E-06

Table 2: Tafel coefficients and Linear Potential Resistance.

	OCP	LPR		TAFEL		POTENTIODYNAMIC	
NaCl %	E (mV) After 10 min	E (mV)	I corr (A/cm²)	E (mV)	I corr (A/cm²)	E (mV)	I corr (A/cm²)
0.035	$-140_{(600s)}$	-111	5.8 E-07	-132	1.8 E-07	-149	5.5 E-07
0.35	-201	-206	2.61 E-06	-190	2.3 E-06	-192	2.5 E-06
3.5	$-236_{(600s)}$	-222	2.23 E-06	-212	2.7 E-06	-210	3.7 E-06

Table 3: Comparison between different corrosion tests.

Shape memory effect

Corrosion effect on shape memory strain recovery was determined using a specially designed bending test described in Section "Experimental - Mechanical Characterization". Fig. 8 shows the typical bending test plot where load is reported as function of deformation angle (proportional to plunger shift). The reported plot was obtained on an uncorroded sample with a maximum plunger shift of 9 mm. In Fig. 9 the results of the cyclic bending test carried on a corroded specimen were reported. The corrosion damage was obtained using a potentiostatic test as described in Section "Experimental-Mechanical characterization". Diamond points indicate the specimen deformation angles under load. They indicate the maximum deformation applied to the specimen and are basically constant and increase only when the plunger shift is increased. Square points show the deformation angle measured when the load is removed. They indicate the residual deformation after the elastic recovery. A little increase in the residual deformation is observed during the first cycle. After cycle 8° residual deformation remains almost constant (see square points) and it increases only when a higher plunger shift is applied. Triangle points show the residual deformation after the shape memory recovery, obtained through a heat treatment at 70 °C for 1 minute. It can be noted that the shape memory recovery significantly decreases during the first ten cycles; the final residual deformation angle decreases from 169° measured after the first cycle to 155°measured at cycle 10. Then it slowly decreases up to the last value of 135° measured after 75° cycle with plunger shift of 7 mm.

The effect of the corrosion damage can be better evaluated through SEM observations of the tensile subjected surface carried out after the bending test and before the shape recovery treatment (Fig. 10). The potentiostatic test resulted in a surface damage mainly located along the microstructure grain boundaries. In these areas the material surface appears hollowed and the second phase, observed often in Fig. 2, is highlighted. The mechanical deformation produces some cracks at the grain boundary starting from the corroded areas. These cracks do not grow with the cyclic mechanical deformation/shape recovery. They increase in number and length only when the mechanical deformation is increased with the application of a higher plunger shift.

Damage signs appear also inside the grain, both as little cracks with a particular V-shape and as well as little voids (see Fig. 10 – i and k). In this case their length do not grow as a function of cycles, but only their quantity.

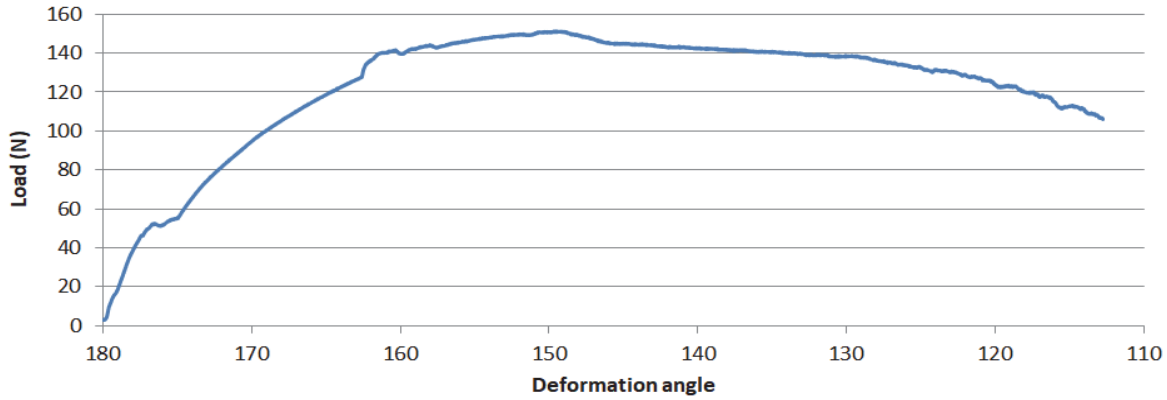

Figure 8: Typical guided bending test plot obtained on a not corroded specimen.

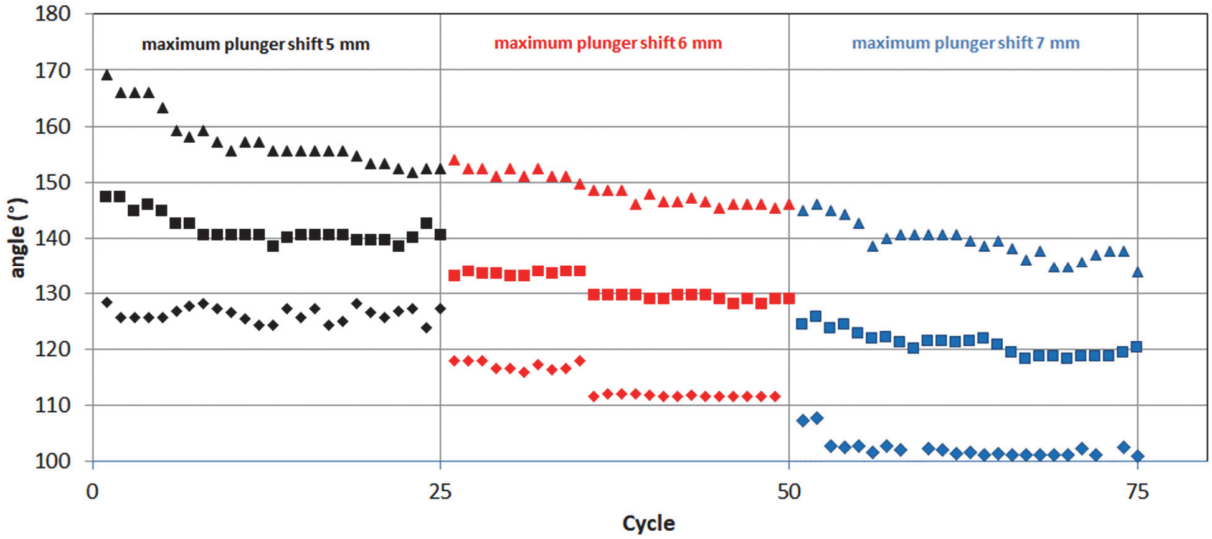

Figure 9: Cyclic guided bending test results on a corroded specimen ◆ deformation angle under load, ■ deformation angle without load (elastic recovery) ▲ residual angle deformation after heating at 70 °C for 1 minute (shape memory recovery).

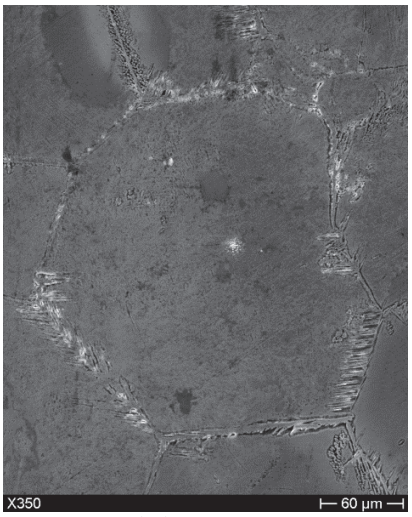

a) As corroded

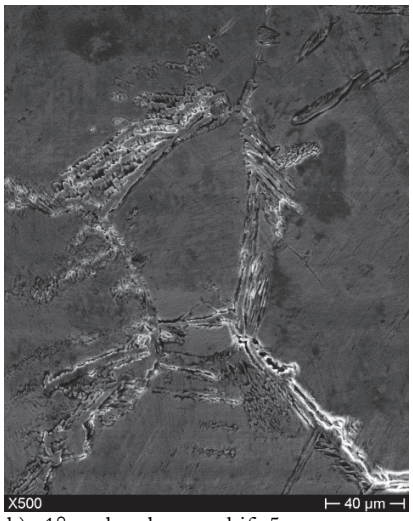

b) 1° cycle, plunger shift 5 mm

c) 5°cycle, plunger shift 5 mm

d) 15° cycle, plunger shift 5 mm

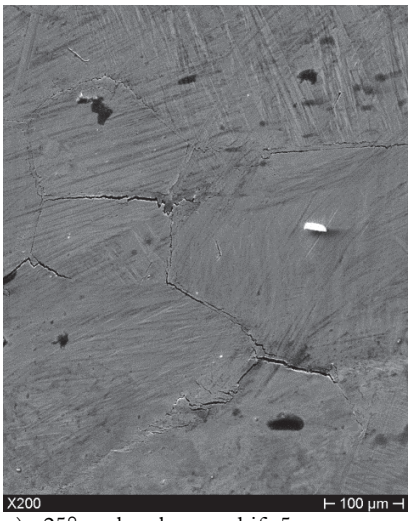

e) 25° cycle, plunger shift 5 mm

f) 35° cycle, plunger shift 6 mm

g) 50 cycle, plunger shift 6 mm

h) 60 cycle, plunger shift 7 mm

i) 75 cycle, plunger shift 7 mm

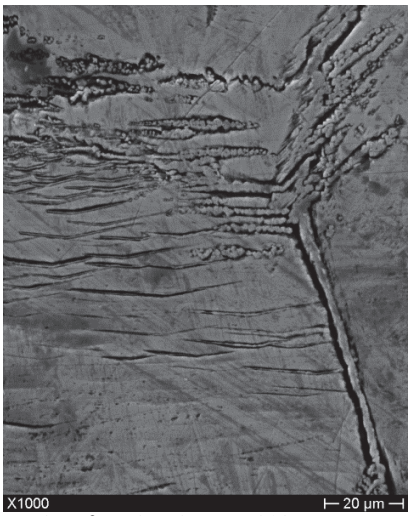

j) l) 15° cycle, plunger shift 5 mm

k) m) 25° cycle, plunger shift 5 mm

l) 50° cycle, plunger shift 6 mm

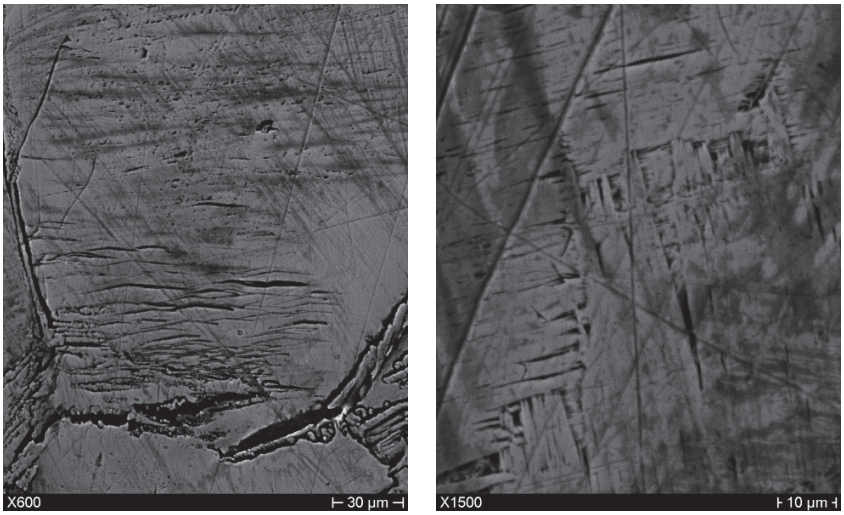

m) 60° cycle, plunger shift 7 mm n) 75° cycle, plunger shift 7 mm

Figure 10: SEM observations of corroded surfaces after mechanical deformation (tensile stressed surfaces).

CONCLUSIONS

The results on corrosion behavior of Cu–Zn-Al alloys obtained by the potentiodynamic analysis, mechanical tests and scanning electron microscopy (SEM-EDS) observations lead to the following conclusions:

- Corrosion data show a behavior of the Cu-Zn-Al SMA tested alloy similar to those of other brass with the same Zn_{eq} level. The corrosion rate (I_{corr}) is dependent on solution concentrations (from 0.035% to 3.5%).
- The effect of corrosion damage on the shape memory alloy is investigated with potentiostatic test and its effect is mainly located in the microstructure grain boundaries. This effect is then compared with cyclic mechanical deformation/shape recovery. The crack produced by mechanical test didn't grow with the cycle applied but only with the application of higher plunger shift. This doesn't imply that the previously damaged SMA exposed to an aggressive environment with or without a superimposed mechanical solicitation can lead to the structural failure of the material.
- It has been observed a reduction of the shape memory recovery capability of a corroded material with the number of the deformation/recovery cycles, but this reduction cannot be directly correlated to the corrosion damage induced on the specimen surfaces. The corrosion damage, predominantly localized on the grain boundary, develops superficial microcracks after the first loading. These microcracks didn't grow neither in length nor in number as function of loading cycle. They increased in length and number only when the loading level (plunger shift) was increased. A future development of the research will be devoted to test this material with a higher number of thermo-mechanical cycles.
- All the data collected in this experimentation could make the Cu-Zn-Al SMA appropriate for engineering applications in coastal environments. The corrosion behavior is like those of other Cu-Zn alloys currently used and the corrosion didn't affect the shape Memory Effect. The observed little reduction of the shape memory recovery is probably linked to a progressive damage accumulation on the interface between the martensite lamellae. However, the mechanical solicitation applied in this experimentation is relatively high and more deep study of the interaction between the SME and the cyclic solicitation will be addressed.

REFERENCES

[1] Fujita, F. (1994). Physics of new materials, Berling Heidelberg, Springer-Verlag.
[2] Wayman, C.M., Otzuka, K. (1998). Shape memory materials.
[3] Yamauchi, K., Ohkata, I., Tsuchiya, K., (2011). Shape Memory and Superelastic Alloys: Technologies and Applications, Woodhead Publishing in Materials, Sawson UK.

[4] Seo, J., Kim, Y., Hu, J.(2015). Pilot Study for Investigating the Cyclic Behavior of Slit Damper Systems with Recentering Shape Memory Alloy (SMA) Bending Bars Used for Seismic Restrainers. Appl. Sci. 5, pp.187–208
[5] Concilio, A., Antonucci, V., Auricchio, F., Lecce, L., Sacco, E. (2011). Shape Memory Alloy Engineering for Aerospace, Structural, and Biomedical Applications, Ed. Butterworth-Heinemann, Second Edition.
[6] Barbarino, S., Saavedra, F., Ajaj, R.M., Dayyani, I., Friswell, M.I. (2014). A review on shape memory alloys with applications to morphing aircraft, Smart Mater. Struct. 23 (2014) 063001.
[7] Alaneme, K. K., Okotete, E. A., (2016). Reconciling viability and cost-effective shape memory alloy options – A review of copper and iron based shape memory metallic systems, Engineering Science and Technology, an International Journal 19, pp. 1582–1592B.
[8] De Filippo, A. Brotzu, S. Natali, (2019) Shape Memory Alloy Applications in Seismic Field, Studia Archaeologica 236, Ed. L'Erma di Bretschneider.
[9] Jani, J. M., Leary, M., Subic, A., Gison, M. A. (2014). A review of shape memory alloy research application and opportunities, J. Mater. Des. 56, pp. 1078-1113.
[10] Coric D. and Zmak, I. (2021). Influence of Ausforming treatment on super elasticity of Cu-Zn-Al Shape Memory Alloy for seismic energy dissipaters, Buildings, 11(1), 22.
[11] Kock, G. (2017). Trends in Oil and Gas Corrosion Research Technologies: Production and Transmission, Woodhead Publishing (2017) Cambridge, England.
[12] Vastag, G., Ivosevic, S., Nikolic, D. (2021). Corrosion Behaviour of Cu-Al-Ni SMA in different coastal environments, Int. J. Electrochem. Sci., 16 (2021).
[13] Iacoviello, F., Di Cocco, V., Natali, S., Brotzu, A. (2018). Grain size and loading conditions influence on fatigue crack propagation in a Cu-Zn-Al shape memory alloy, Int. J. Fatigue 115, pp. 27-34
[14] Di Cocco, V., Iacoviello, F., Natali, S., Brotzu, A. (2015). Fatigue Crack micromechanisms in a Cu-Zn-Al shape memory alloy with pseudo-elastic behavior, Frattura ed Integrità Strutturale, 9 (34) pp. 415-421.
[15] Di Cocco, V., Iacoviello, F., Carlino, F., Natali, S. (2018). Grain size influence on fatigue behaviour in a CuZnAl PE SMA, Proc. Struct. Integrity 13, pp. 204-209.